Supplementary Information for:

Structural and Morphological Changes of Breast Cancer Cells Induced by Iron (II) Complexes

Janske Nel [a†], *David Siniscalco* [b†], *Cécilia Hognon* [c†], *Mathilde Bouché* [d], *Nadége Touche* [e*], *Émilie Brunner* [e], *Philippe C. Gros* [d], *Antonio Monari* [c,f*], *Stéphanie Grandemange* [e*], *Grégory Francius*[b*]

[a] Université de Lorraine, LIBio, F-54000, Nancy, France

[b] Université de Lorraine and CNRS. LPCME UMR 7564, F-54000 Nancy, France

[c] Université de Lorraine and CNRS, LPCT UMR 7019, F-54000 Nancy, France

[d] Université de Lorraine and CNRS, L2CM UMR 7053, F-54000, Nancy, France

[e] Université de Lorraine and CNRS, CRAN UMR 7039, F-54000 Nancy, France

[f] Université de Paris, ITODYS, CNRS, F-75006, Paris, France

[†] These authors contributed equally to this work

[*] Corresponding authors

UV-visible spectroscopy measurements for aggregation of AIM

To ascertain the stability of AIM 2/3, and the absence of aggregation phenomenon in the specific conditions used in the contribution, two test experiments were performed at 10x the working concentration (*i.e.* 20 µM) and analyzed by UV-visible spectroscopy. AIM 3 was used as the model molecule due to the similarities between AIM 2 and 3. First, to ascertain the absence of solvatochromism of the metal-to-ligand charge transfer peak that is characteristic of the stability of AIM 3, and ensure the absence of aggregation in cell culture medium, a 20 µM solution of AIM3 was prepared in fully supplemented DMEM/Nutrient Mix F-12 cell culture media (as described in the Cell Culture section of the Methods and Materials), analyzed by UV-visible spectroscopy at 25 °C and compared to control solutions of AIM 3 at 20 µM in either ethanol or deionized H_2O where AIM 3 is fully soluble (**Figure S1 a**). The spectrum in cell culture medium shows neither shift nor broadening of the metal-to-ligand charge transfer absorption peak compared to the control solvents, indicating that AIM 3 is fully soluble in cell culture medium and does not aggregate at 20 µM. A second experiment was performed to ensure the stability of AIM 3 toward incubation in cell culture medium (**Figure S1 b**). To do so, a 20 µM stock solution of AIM 3 was prepared in ethanol (5 mM) and diluted to 20 µM in fully supplemented DMEM/Nutrient Mix F-12 cell culture medium. The samples were then incubated at 37 °C on a Thermomixer under 1000 rpm stirring for the indicated times, *i.e.* 0, 24, 48, 72 and 96 h. UV-vis spectroscopy was performed at 25 °C at each time point. The metal-to-ligand charge transfer band showed neither a decrease in intensity at longer incubation time points nor broadening, indicating the high stability of AIM 3 toward degradation or aggregation in cell culture medium. Overall, both experiments indicate that the AIM 3 working concentration in this study (2 µM) is perfectly suited to maintain high stability to further pursue *in cellulo* experiments.

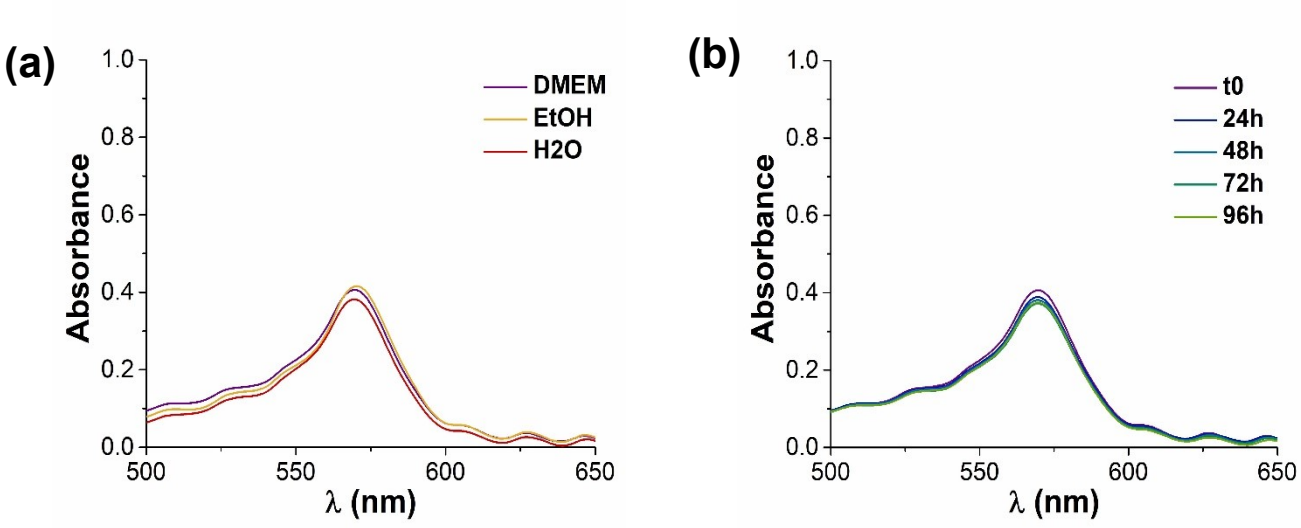

Figure S1. UV-vis spectroscopy data concerning the stability and absence of aggregation of AIM 3 at 20 μM in (a) DMEM/Nutrient Mix F-12 cell culture media compared to solvents showing high solubilization properties toward AIM3 (*i.e.* ethanol or water), and (b) in DMEM/Nutrient Mix F-12 cell culture media over time (0 – 96 h, 37°C). The sharp and intense peak in both Figures indicates no aggregation of the AIM complexes.

Bottom effect correction applied to AFM

All experimental force-distance curves were processed using MATLAB algorithm described by Polyakov et al. according the following equation:

$$F = \frac{8E\tan\theta}{3\pi}\delta^2 \cdot f_{BECC}$$

Where θ is the semi-top angle of the AFM-tip and f_{BECC} is the bottom effect cone correction function. Many correction functions are described in literature, notably by Garcia et al. [1] and Gavara et al. [2] for the analysis of cells and membrane nanomechanical properties.

In the present work we used the bottom effect cone correction function described by Gavara et al. according to the following equation:

$$f_{BECC} = 1 + 0.361\chi + 50.5201\chi^2 + o(\chi^3)\ with\ \chi = 0.315\left(\frac{\delta}{h}\right)$$

Where δ and *h* correspond to the indentation and the sample thickness, respectively.

Even though, the correction function described by Gavara et al. is less accurate and does not converge with the one described by Garcia et al., the functions are similar with non-significant differences for small indentations (*i.e.* when $\delta/h < 0.2$).

The bottom effect correction function described by Garcia et al. follow the equation below:

$$f_{BECC} = 1 + 0.721\chi + 0.650\chi^2 + 0.491\chi^3 + 0.225\chi^4\ with\ \chi = 0.315\left(\frac{\delta}{h}\right)$$

As illustrated by **Figure S2** the differences between the two corrective functions does not exceed 30 % in the range of our analysis in terms of mechanical stress ($\delta/h < 0.4$). We underline that Garcia corrective model is the most suitable/accurate model whatever the range of cell deformation while Gavara's one remains valid only for small cell deformation (*i.e.* $\delta/h < 0.2$). Gavara's correction applied to our data leads about 10% relative error on the mean values as reported in **Table 1**.

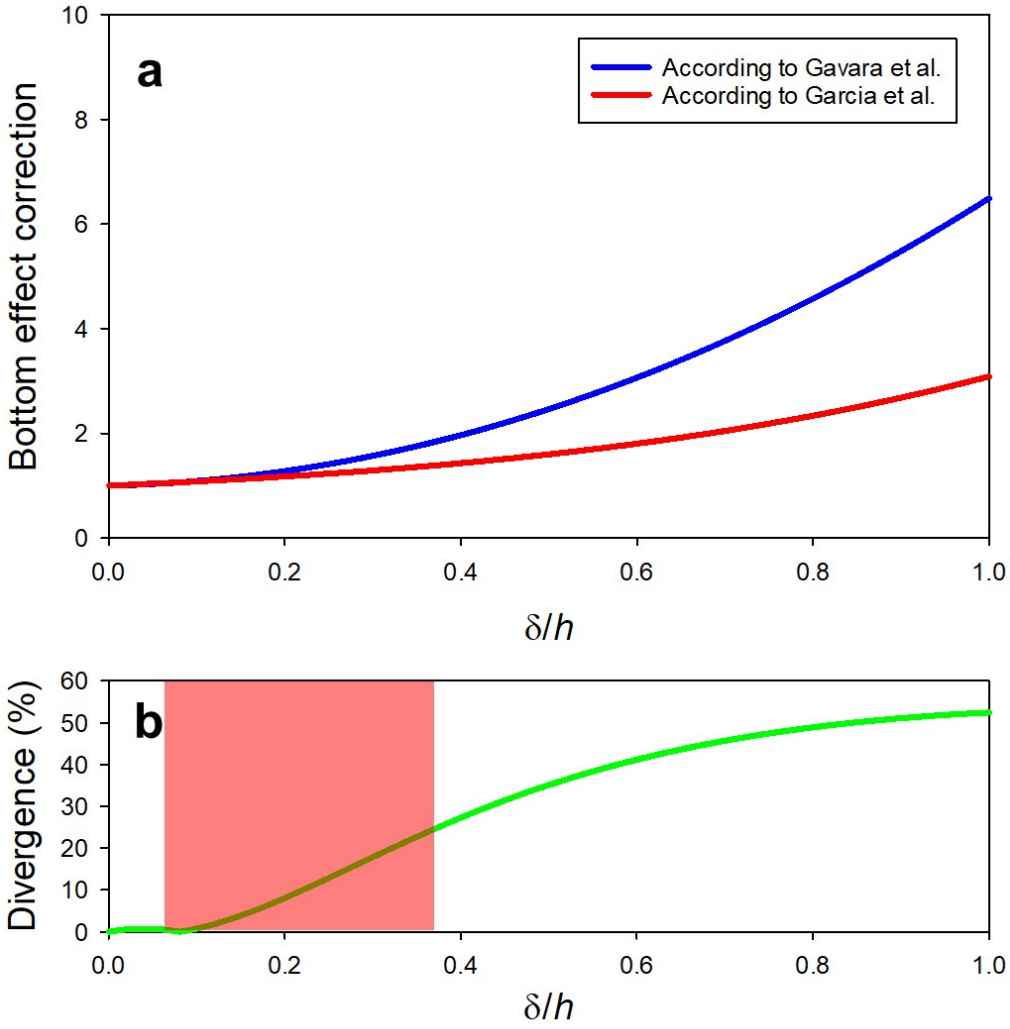

Figure S2. Evolution of the bottom effect cone correction functions with the mechanical stress according to equations described by Gavara et al (blue line) and Garcia et al (red line) for the AFM-tip geometry used in this work. Noticed that the divergence between the two corrective functions is illustrated by the green line in the lower panel. The pink zone corresponding to the range of our mechanical analysis evidenced that differences between the two corrections is lower than 30 % that is negligible as regarding the width of mechanical distributions reported in Figure 4 in the main manuscript and Figure S3 in the Supplementary Information.

All data exhibited an important width in their corresponding statistic distribution. Such width could originate from cell heterogeneity and variations in contact geometry during experiments. Given this important width in stiffness distribution (from 0 up to 30 kPa) and the huge data set (at least 3000 values per condition) the systematic errors on measurements don't have a significant effect on the global results and trends depicted here.

Analysis of experimental curves and individual cell stiffness extraction

All experimental force curves were analyzed according to the model described in the manuscript including the bottom effect correction function. Our experimental data were well fitted with the model as illustrated by **Figure S3**.

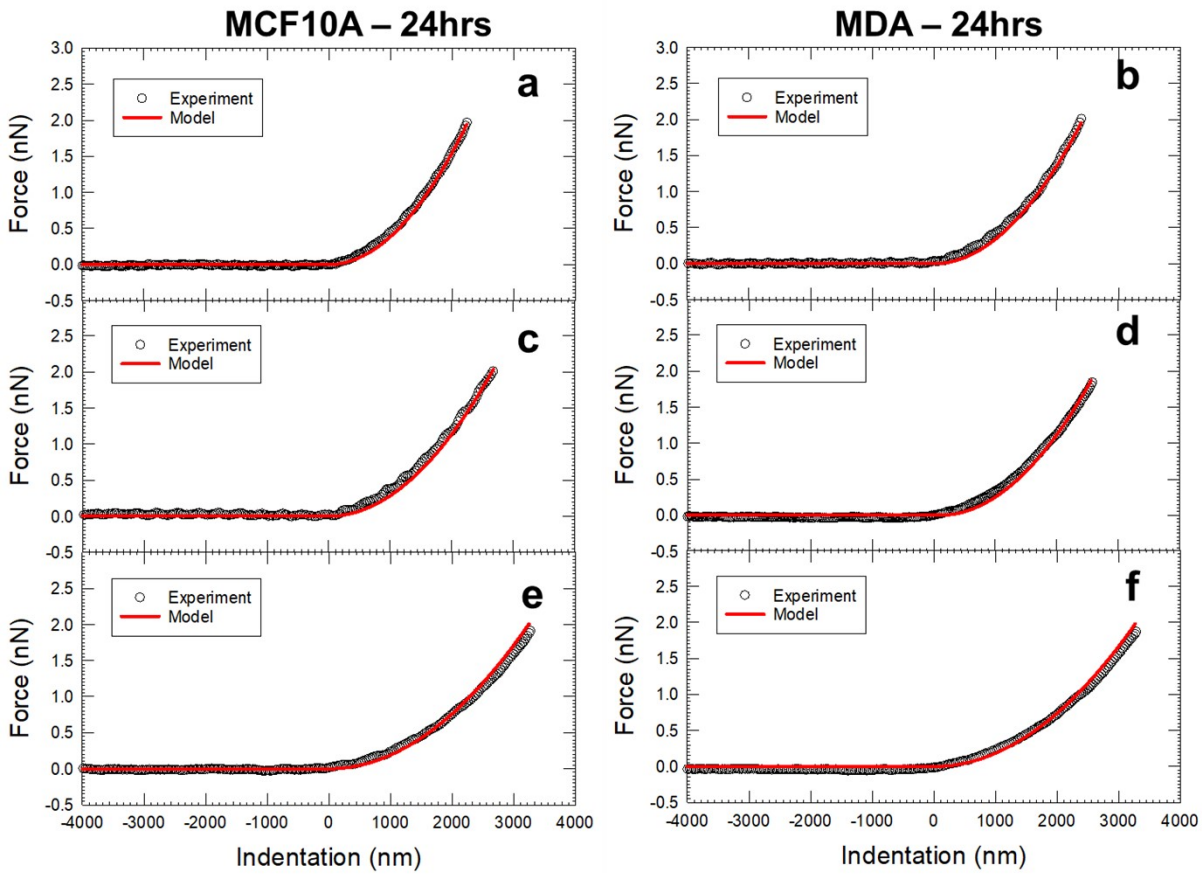

Figure S3. Representative force-indentation curves recorded on living MCF10A and MDA-MB-231 cells before (**a & b**) and after treatments with AIM 2 (**c & d**) and with AIM 3 (**e & f**). Experimental data and theoretical fitting correspond to the white circles and the red lines respectively.

Mechanical properties of individual cells were determined from the analysis of the Force-Volume Images (FVI). Each FVI contained at least 4 cells and consists of a grid of 50 by 50 force curves allows the generation of an elasticity map as illustrated by **Figure S4**. Each elasticity map is further analyzed to extract only the stiffness for each cell by comparing height profile image and its corresponding elasticity map. All truncated cells or located in the edges of the FVI are excluded from the analysis. Only entire cells are considered for the study.

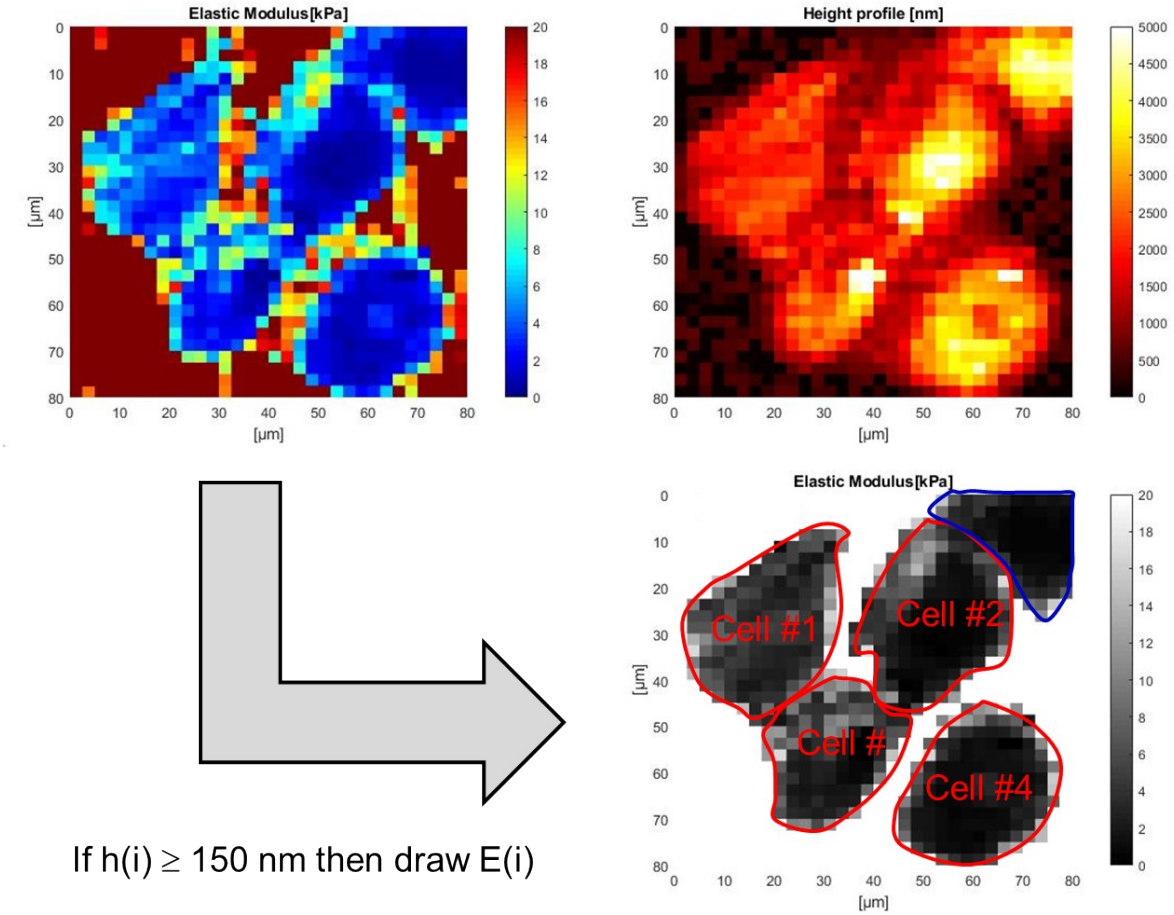

Figure S4. Schematic representation of individual cell stiffness extraction from the Force Volume Images using a MATLAB algorithm using image processing toolbox (only red surrounded cells are take into account for our calculations while blue surrounded cells are excluded from the analysis).

The statistic distributions of whole set of individual cell stiffness (see **Figure S5** and **Figure S6**) are pooled according to their treatment condition and reported in global statistic distribution in the main text (see **Figure 4**).

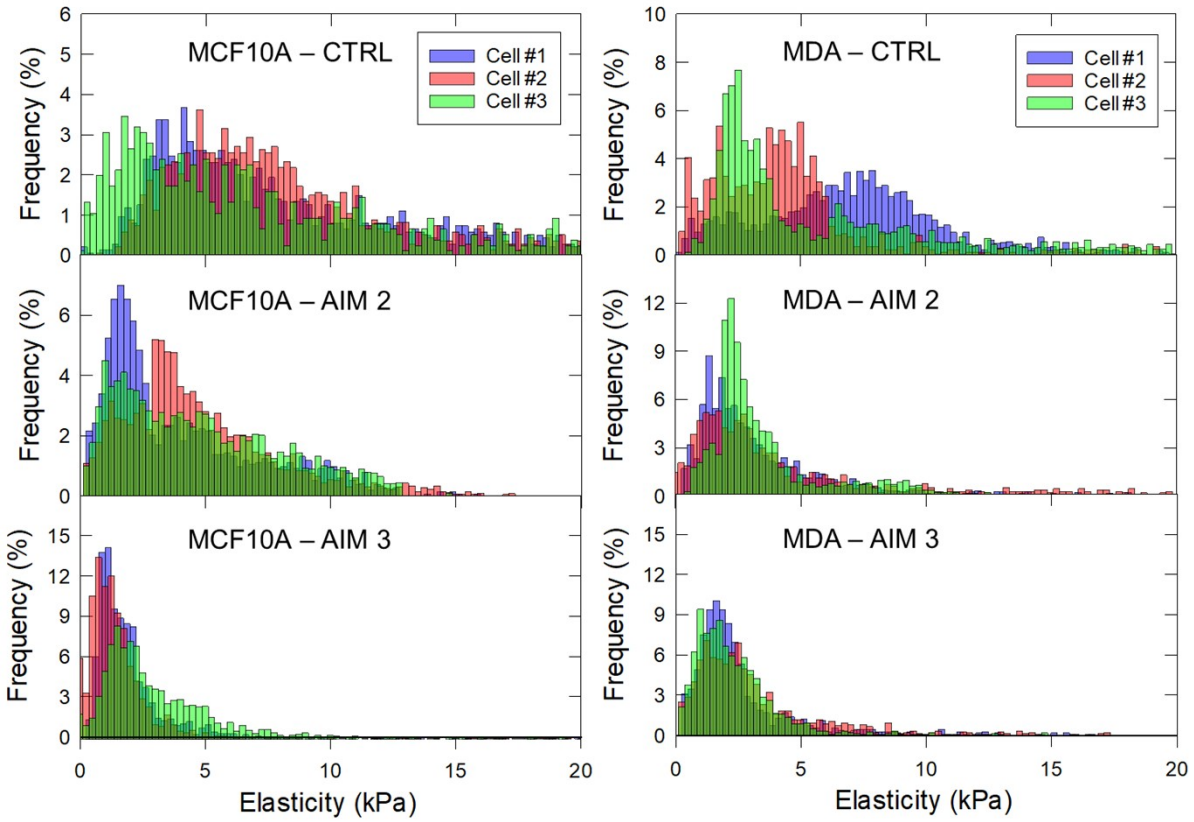

Figure S5. Examples of statistic distribution of stiffness of 3 cells at 96 h before (CTRL) and after treatment with AIM complexes.

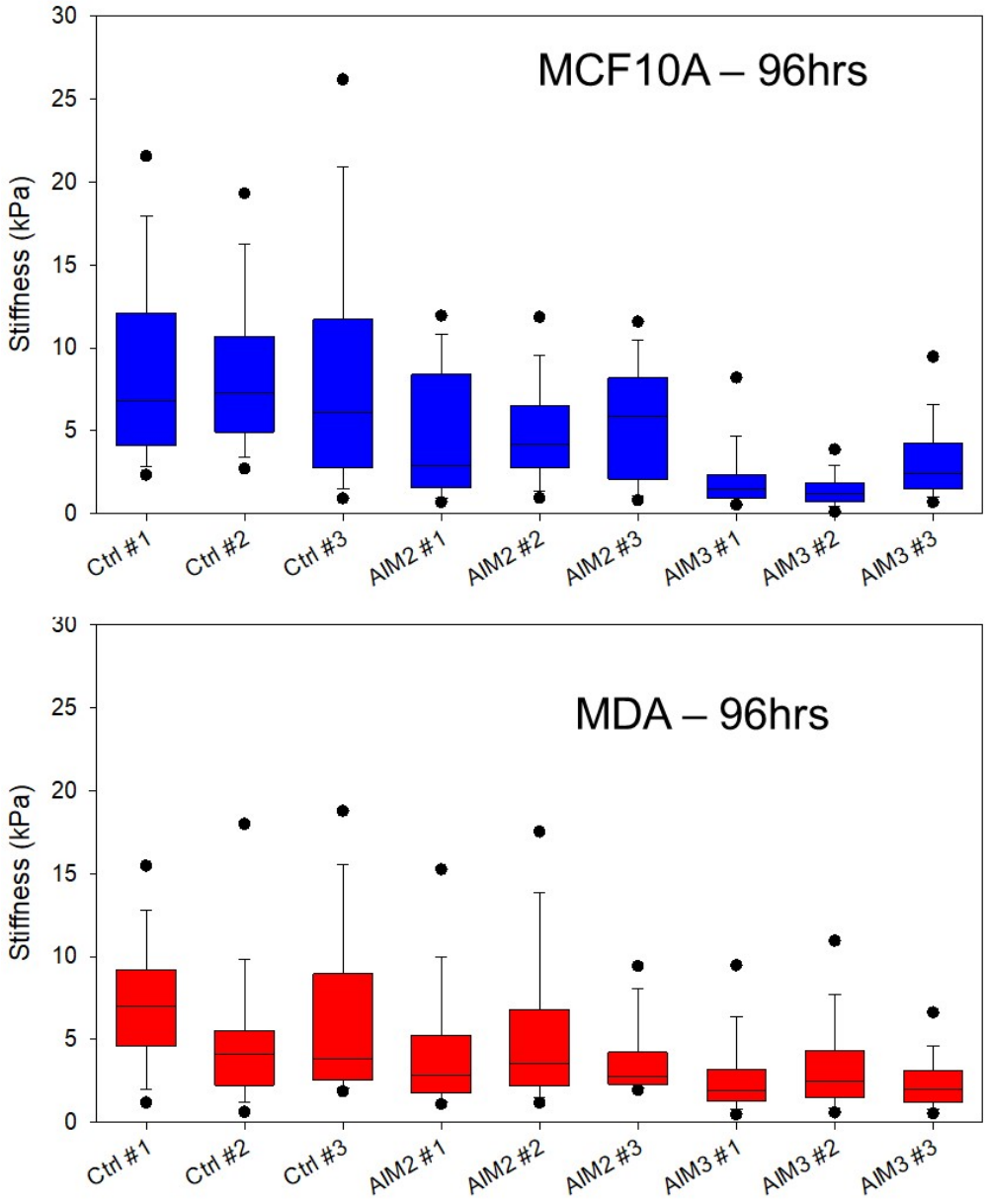

Figure S6. Examples of box-and-whisker plot graphics of individual stiffness of 3 cells at 96 h and before (CTRL) and after treatment with AIM complexes.

Real-time morphology evolution of SLB

The morphological changes of the DPPC/POPC (3:1) membranes were monitored in buffer solution after addition of either AIM 2 or AIM 3, at a final concentration of 50 µM over 20 µm ⊗ 20 µm area. To get more resolution and accuracy in our investigation, we show topographic images over 4 µm ⊗ 4 µm areas from the same images as **Figure 3**.

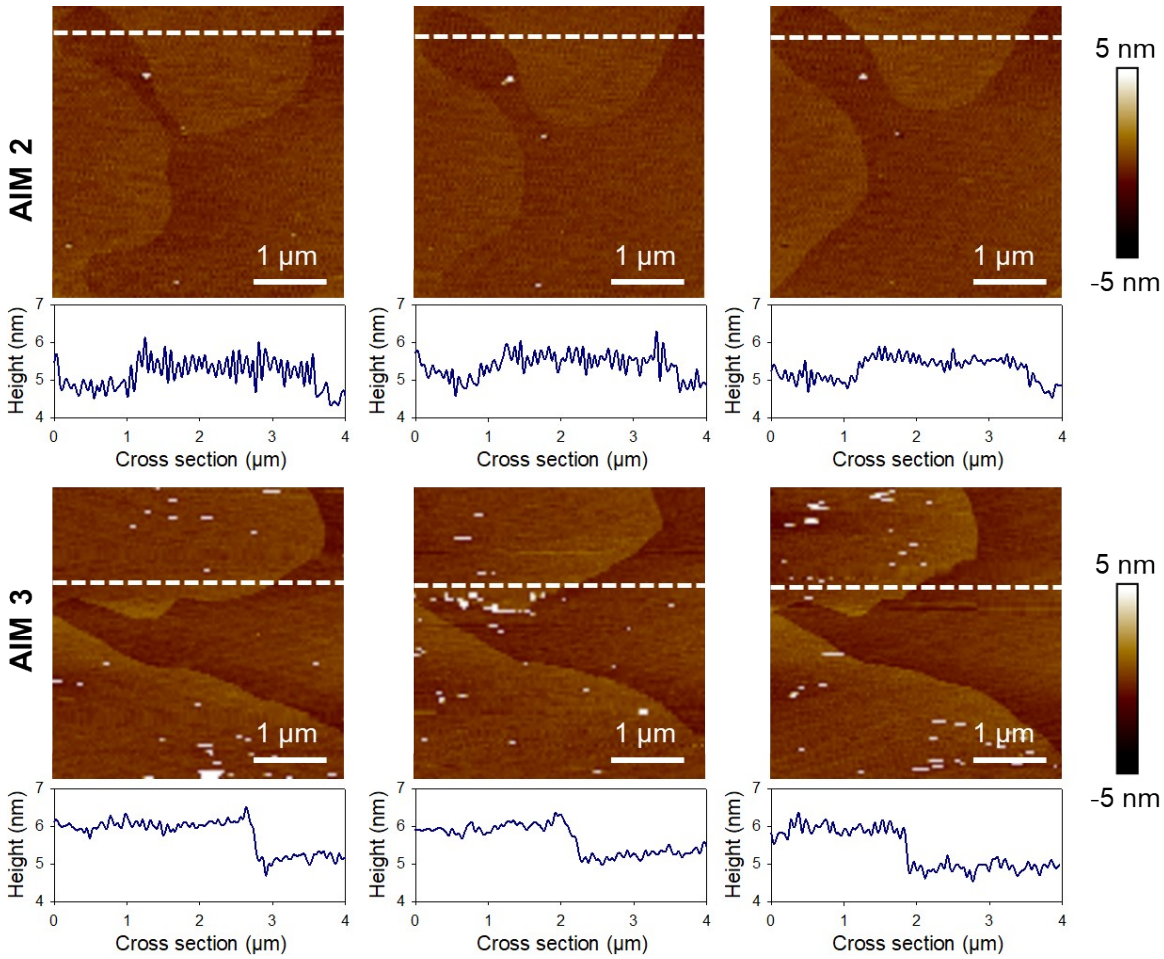

Figure S7. AFM images monitoring the real time evolution of DPPC/POPC SLB under the effects of either AIM 2 or AIM 3 after 0, 30 and 60 mins. Vertical cross-section indicating height measured at dashed line of images. Image scale bar is set to 1 µm.

Table S1. Number of aggregates after AIM 2/3 exposure on the SLB surfaces for 0, 30 or 60 min.

Number of aggregates (AFM images analysis for SLB exposed to AIM2)			
Time (min)	DPPC domain (≈280 μm²)	POPC domain (≈120 μm²)	Total area (≈400 μm²)
0	85	47	132
30	92	64	156
60	63	62	125

Number of aggregates (AFM images analysis for SLB exposed to AIM3)			
Time (min)	DPPC domain (≈90 μm²)	POPC domain (≈310 μm²)	Total area (≈400 μm²)
0	90	40	130
30	139	56	195
60	230	27	257

Statistical analysis of cells mechanical stiffness after AIM 2/3 complexes treatment

Given the important width of cell stiffness distribution upon the different metallodrugs treatments, we performed an ANOVA analysis to compare each condition for MCF 10A and MDA-MB-231 cells. Results reported in **Table S2** evidenced that even though the stiffness distributions are broad and can overlap, there are significant differences between control cells and those subjected to the different metallodrugs treatment.

Table S2. Associated ANOVA analysis of the stiffness measurements of MCF 10A and MDA-MD-231 cells after 2 µM treatment with AIM 2/3 at either 24 or 96 h.

ANOVA analysis (MCF 10A after 24 h)

Comparison	**Difference of Ranks**	**Q**	**P**	**P<0.050**
Control vs AIM 2	1446.45	24.58	<0.001	Yes
Control vs AIM 3	2701.804	37.866	<0.001	Yes
AIM 2 vs AIM 3	1255.354	16.867	<0.001	Yes

ANOVA analysis (MCF 10A after 96 h)

Comparison	**Difference of Ranks**	**Q**	**P**	**P<0.050**
Control vs AIM 2	1010.268	8.269	<0.001	Yes
Control vs AIM 3	4843.566	39.114	<0.001	Yes
AIM 2 vs AIM 3	3833.299	44.811	<0.001	Yes

ANOVA analysis (MDA-MB-231 after 24 h)

Comparison	**Difference of Ranks**	**Q**	**P**	**P<0.050**
Control vs AIM 2	430.526	6.712	<0.001	Yes
Control vs AIM 3	806.92	12.979	<0.001	Yes
AIM 2 vs AIM 3	376.395	6.324	<0.001	Yes

ANOVA analysis (MDA-MB-231 after 96 h)

Comparison	Difference of Ranks	Q	P	P<0.050
Control vs AIM 2	2549.628	22.963	<0.001	Yes
Control vs AIM 3	436.71	4.243	<0.001	Yes
AIM 2 vs AIM 3	2112.918	21.672	<0.001	Yes

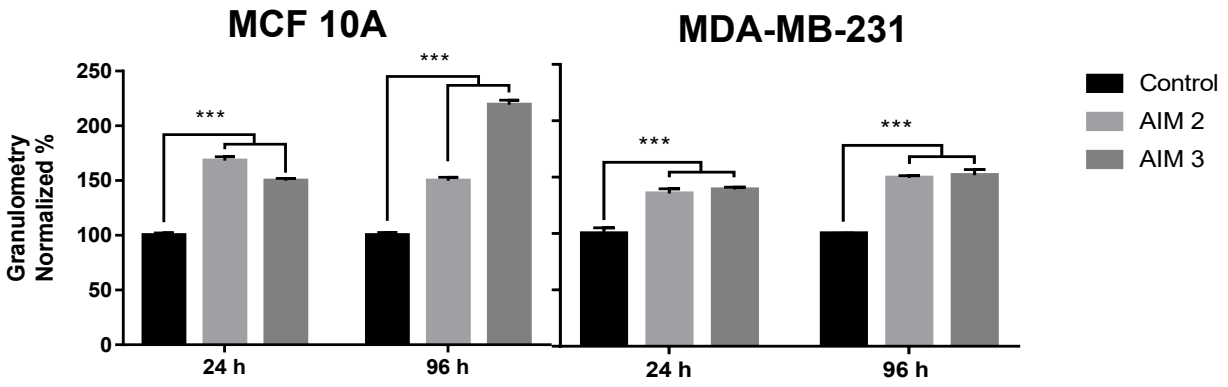

Figure S8. The effect of iron (II)-based complexes on the granulometry of MCF 10A and MDA-MB-231 cells. Cells were treated with 2 μM AIM 2 or AIM 3 for 24 or 96 h and analysed by flow cytometry to determine the effect of the metallodrugs on granulometry. Results are shown as normalized percentage with ±SD with untreated cells at each time point

Table S3. Flow cytometry results, before percentage normalization, indicating the effect of AIM 2 and AIM 3 on the size and granulometry of MCF 10A and MDA-MB-231 after 24 or 96 h. All experiments were performed in triplicate. Results acquired as x 10^4.

Granulometry (mean, ±SD)			Granulometry (mean, ±SD)		
Treatment	**24 h**	**96 h**	**24 h**	**96 h**	**Treatment**
Control	15.44 ±0.34	21.71 ±0.54	Control	14.46 ±0.73	18.17 ±0.05
AIM 2	25.97 ±0.95	47.97 ±1.49	AIM 2	19.61 ±0.81	27.17 ±0.52
AIM 3	23.15 ±0.50	47.60 ±1.93	AIM 3	20.10 ±0.44	27.59 ±1.36

Wound healing assay

To visualize the migration ability of MCF 10A and MDA-MB-231 cells after 24 or 72 h treatment with AIM 2/3, wound healing migration assays were performed. To ensure the observation of cellular migration and not proliferation, each cell line was seeded at a specific density for each treatment time to ensure the appropriate confluency. For the 24 h treatment with AIM 2/3, MCF 10A and MDA-MB-231 cells were seeded at a density of 2.1 x 10^4 or 3.6 x 10^4 cells/cm² respectively into 6 cm cell culture plates (Nunclon Delta Surface, Thermo Fisher Scientific, Roskilde, Denmark) and incubated overnight to allow for cell attachment. Subsequently, cells were treated with 2 µM (w/v) of AIM 2/3 for 24 h. Following this, a sterile 1000 µL pipette tip was used to create a scratch in the cell monolayer. Cells were washed twice with PBS to ensure scratched cells did not reattach and fresh medium was applied with no AIM. Light microscopy images were taken at 0, 6, 24 and 48 h after the scratch with an inverted microscope (Motic AE31, France) using a ×40 objective and collected with a digital camera (Moticam 2300, France). For the 72 h experiment, the control MCF 10A and MDA-MB-231 cells were seeded at a density of 1.3 x 10^4 or 3.9 x 10^4 cells/cm² respectively into 15 cm cell culture plates (Nunclon Delta Surface, Thermo Fisher Scientific, Roskilde, Denmark), whilst the experimental cells were seeded at 3.1 x 10^4 or 6.1 x 10^4 cells/cm² respectively. After incubating the cells overnight to allow for cell attachment, the experimental cells were treated with 2 µM (w/v) of AIM 2/3 for 72 h. After 72 h, the control and treated MCF 10A and MDA-MB-231 cells were trypsinated and seeded at a density of 2.1 x 10^4 or 3.6 x 10^4 cells/cm² respectively into 6 cm cell culture plates and incubated overnight. A sterile 1000 µL pipette tip was used to create a scratch in the cell monolayer. Cells were washed twice with PBS and fresh medium was applied with no AIM. Images were taken at 0, 6, 24 and 48 h after the scratch with the equipment previously described. Each experiment was repeated twice.

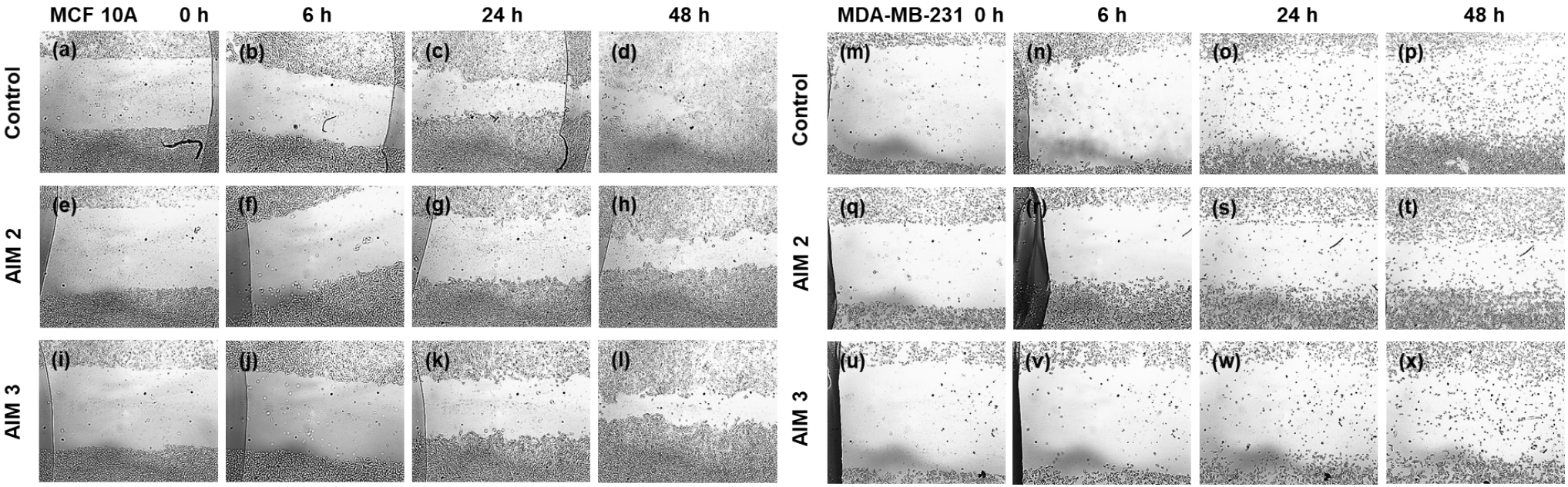

Figure S9. Wound healing scratch test assay images of MCF 10A (**a – l**) and MDA-MB-231 (**m – x**) cells after 24 h of AIM 2 or AIM 3 pre-treatments at 40X magnification. The ability of the cells to migrate, after a scratch was applied to the monolayer, was monitored immediately after at 0, 6, 24 and 48 h.

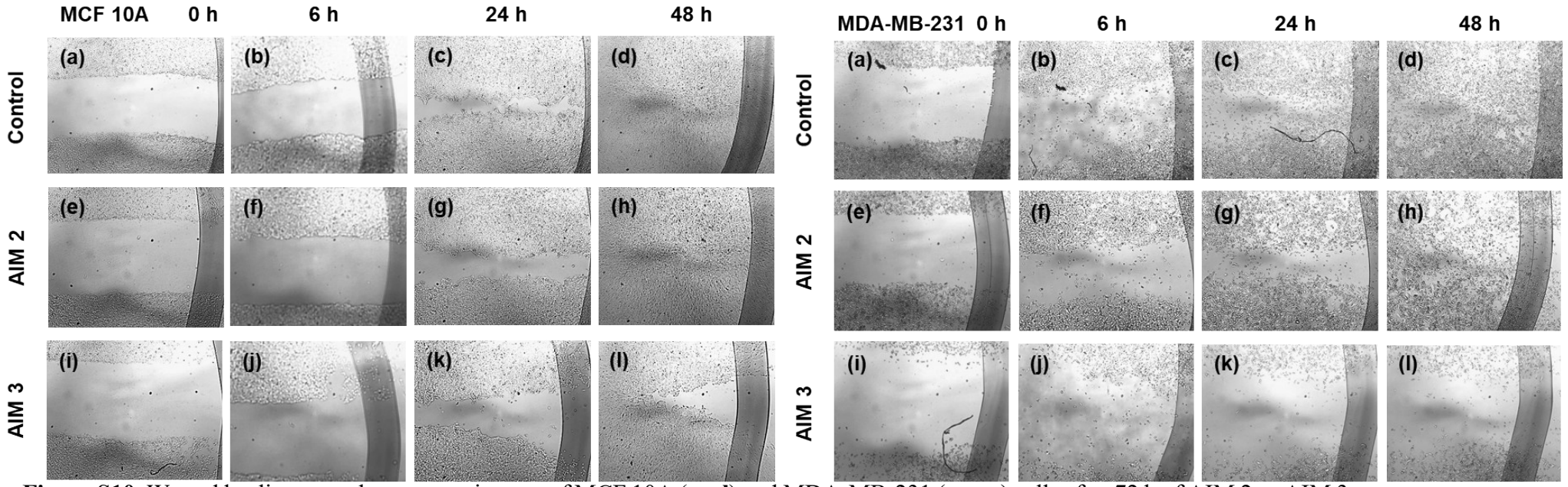

Figure S10. Wound healing scratch test assay images of MCF 10A (**a – l**) and MDA-MB-231 (**m – x**) cells after 72 h of AIM 2 or AIM 3 pre-treatments at 40X magnification. The ability of the cells to migrate, after a scratch was applied to the monolayer, was monitored immediately after at 0, 6, 24 and 48 h.

References used in Supplementary Information:

(1) Garcia, P. D.; Garcia, R. Determination of the Viscoelastic Properties of a Single Cell Cultured on a Rigid Support by Force Microscopy. *Nanoscale* **2018**, *10* (42), 19799–19809. https://doi.org/10.1039/C8NR05899G.

(2) Gavara, N.; Chadwick, R. S. Determination of the Elastic Moduli of Thin Samples and Adherent Cells Using Conical Atomic Force Microscope Tips. *Nat. Nanotechnol.* **2012**, *7* (11), 733–736. https://doi.org/10.1038/nnano.2012.163.